SAND2018-9496R

Standardizing solar-to-hydrogen efficiency calculations for the evaluation of new water splitting materials

Marcus A. Battraw[1,2] Kevin J. Albrecht[3] and Anthony H. McDaniel[4]

[1]*Department of Engineering, CSU Chico, Chico, California, 95929, USA*

[2]*Department of Mathematics, CSU Chico, Chico, California, 95929, USA*

[3]*Sandia National Laboratories, 1515 Eubank SE, 87123, Albuquerque, USA*

[4]*Sandia National Laboratories, 7011 East Avenue, 94550, Livermore, USA*

Solar thermochemical hydrogen (STCH) production is one avenue for converting sunlight into hydrogen through concentrating solar thermal technology. STCH is a two-step redox process that begins with concentrated sunlight to thermally reduce a metal oxide around 1500 ℃ leaving it in an oxygen deficient form. Subsequent exposure of the reduced metal oxide to steam at lower temperature reoxidizes the material and produces hydrogen. The efficiency of this process is dependent on the metal oxide material thermodynamic properties and cycle operating conditions. Numerous thermodynamic modeling efforts to date have been developed around the metal-oxide ceria (CeO_2). However, the thermodynamics are insufficient for achieving efficiency and cost targets specified by the Department of Energy. Therefore, new materials need to be developed and compared using a standard tool for determining their potential solar-to-hydrogen efficiency. In this paper, a modeling approach to standardize the calculation method for system-level solar-to-hydrogen efficiency is presented. The model can be easily modified to evaluate new material thermodynamic properties or modified to reconfigure or replace system component models.

I. INTRODUCTION

Producing renewable chemical fuels as an alternative to fossil-based resources has the potential to decarbonize the transportation fleet. However, to make renewable fuels a viable alternative the efficiency and subsequent cost of converting a renewable resource into a useable chemical fuel needs to be on par with that of the nonrenewable processes. Three different approaches for the renewable production of hydrogen are being studied including electrochemical, photochemical and thermochemical methods. The electrochemical approach directly uses electrical energy to drive an electrolysis cell where electrocatalysts split the water molecule and the resultant oxygen ions or protons are transported across an ion transport membrane to produce and/or purify the hydrogen. The photochemical (or more aptly photoelectrochemical) method directly uses light at a given wavelength to create charge separation in a semiconductor where chemical reactions with charge carriers moderated by an electrocatalysts split the water molecule to produce hydrogen. The final approach, which is studied in this paper, is a thermochemical process that utilizes heat energy to drive a family of chemical reactions that net water splitting and hydrogen production.

Solar thermochemical hydrogen (STCH) production uses the heat energy collected from concentrating sunlight to create a thermodynamically favorable condition for the production of hydrogen. STCH typically uses a two-step cyclic process for converting solar thermal energy to hydrogen, which is depicted in equations (1) and (2). The first step in the process reduces a metal-oxide at temperatures around 1500 °C and low oxygen partial pressure, which can be achieved with concentrated sunlight and vacuum pumping to reduce the total pressure in the reactor. The second step exposes the oxygen deficient material to steam where at lower temperatures it reoxidizes producing hydrogen.

$$MO_x \xrightarrow{Solar\ Heat} MO_{x-\delta} + \frac{\delta}{2} O_2 \quad (1)$$

$$MO_{x-\delta} + \delta H_2O \rightarrow MO_x + \delta H_2 \quad (2)$$

The efficiency of this two-step process is dependent on the material thermodynamic properties and cycle operating conditions. In order to assess the solar-to-hydrogen efficiency, the entire system must be modeled including the two chemical reactors as well as balance-of-plant components to understand the design trade-offs between system operating conditions, material thermodynamics and the resulting energy parasitics and losses that occur. The cyclic process with energy and gas flows is depicted in a simple process flow diagram in FIG. 1. Potential loss mechanisms for this system include solar collection inefficiencies from high-temperature operation, electrical energy consumption from a vacuum pump to create the reducing condition, thermal energy requirement to create steam, heat rejection due to operating the two steps at different temperatures, and electrical energy consumption for gas and particle transport. Therefore, a system model that captures the chemical equilibrium of the solid and gas phases as well as the thermal integration through recuperative heat exchangers must be developed and used to predict the limitations of solar-to-hydrogen efficiency for a given metal oxide.

Numerous studies have been conducted using this two-step redox process as a foundation for both the production of hydrogen and carbon monoxide. Limitations to this process have been discussed by Bulfin et *al.*[5]. To increase the efficiency of the redox process low oxygen partial pressure is desired during reduction of the metal oxide. Reducing conditions can be generated with the introduction of a sweep gas or vacuum pump, which both result in an electrical energy parasitic. An in-depth study taking into account the ceria oxygen release characteristics and sweeping gas oxygen uptake was completed by Brendelberger et *al.*[6], reporting efficiencies less than 20%. In the

previous work being conducted a redox process for the extraction of chemical fuels utilizing sunlight is being studied with the goal to overcome limitations and increase efficiency or storage related applications.

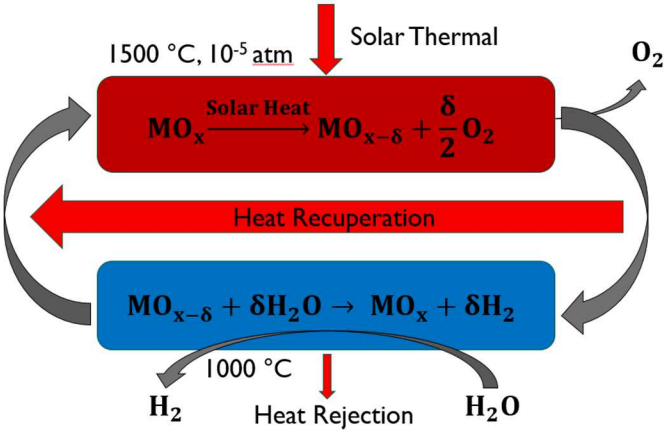

FIG. 1. Schematic of the two-step redox process with heat and gas flows depicting the use of concentrated sunlight to produce chemical fuels.

Since current material thermodynamics have been found to be insufficient for achieving efficiencies and cost targets specified by the Department of Energy, new materials need to be developed that reduce at lower temperatures without negatively impacting the other system parasitics. To assess the performance of new material formulations, a standard tool for determining their potential solar-to-hydrogen efficiency is essential. Furthermore, the model must be capable of being reconfigured and modified as reactor design and advance system configurations are developed. In the following sections, the component models of a baseline two-step STCH system are developed and used to calculate the solar-to-hydrogen efficiency with ceria.

II. Model Approach

A component based model is a powerful tool for many multistep systems. Therefore, the model presented is implemented in OpenModelica, an object-oriented modeling language. With

research in new metal oxides materials and reactor technologies, individual components can be updated and the model reconfigured with ease. Connectors are made and added to each component to allow for data transfer where multiple components can be connected to define a process flow model of the complete system.

The process flow diagram of the baseline two-step STCH system is depicted in FIG. 2 including all of the necessary balance-of-plant components. Solar energy harnessed from concentrated sunlight increases the temperature of the metal oxide inside the solar reduction receiver to approximately 1500 °C and vacuum pumping of the evolved oxygen reduces the total pressure in the reactor to approximately 1-100 Pa. Inside the solar reactor the metal oxide simultaneously experiences high temperature and low oxygen partial pressure, which generates a reducing condition such that some of the oxygen in the metal oxide is evolved into the gas phase. The reduced metal oxide is then transferred to the water splitting reactor where it is exposed to steam at a lower temperature (< 1500 °C) and ambient pressure. This drop in temperature and increase in pressure shifts the thermodynamic equilibrium of the metal oxide to an oxidizing condition. The metal oxide reoxidizes by stripping the oxygen atom from a water molecule to produce hydrogen. In between the two reactors a particle recuperative heat exchanger is implemented to allow for some of the sensible heat to be recuperated that would otherwise be rejected, or made up by the solar input to create the temperature difference between the reactors. Steam generation for the water splitting reactor is another important aspect of the system which can be at least partially performed by the exotherm of the oxidation in the water splitting reactor and recuperation of heat in the gas leaving the water splitting reactor. Since only part of the steam introduced to the water splitting reactor is converted to hydrogen it is necessary to condense the excess steam to separate the hydrogen where the liquid water can be recycled back to the boiler.

Finally, blowers and particle lifts are necessary to provide the required gas and particle flows in the system.

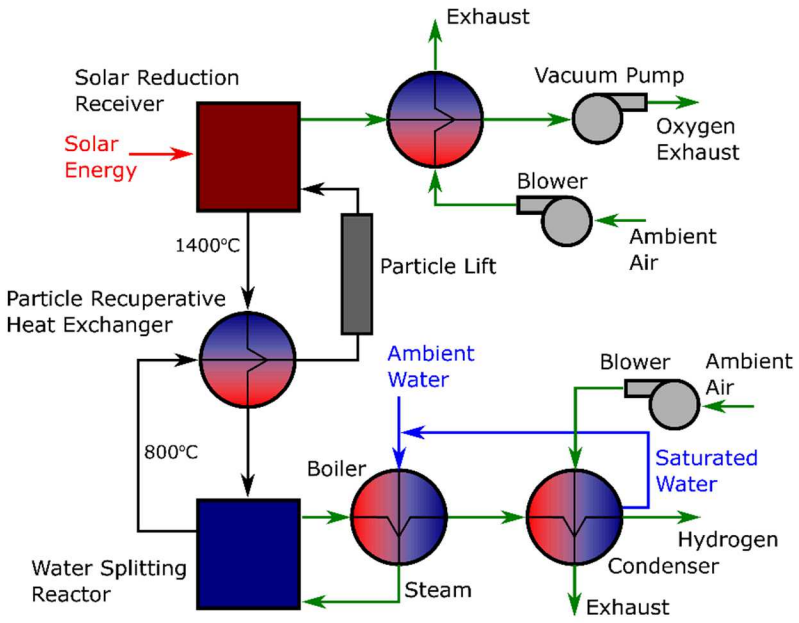

FIG. 2 . Process flow diagram of the baseline two-step STCH system including the reactors, heat exchangers, and balance-of-plant components.

The process flow diagram and explanation above motivates the component models that need to be developed to calculate system efficiency. Most notably, reactor models for representing the reduction and water splitting steps need to be developed that can appropriately capture the extent of reaction based on chemical equilibrium and energy requirement as a function of operating conditions. A radiation heat transfer model is also needed for the solar receiver to determine the efficiency of the solar collection process. In addition, heat exchangers for both the gas and solid phases are needed to perform heat recuperation, addition, and rejection. Specialized versions of the heat exchangers are needed to capture phase change of the water component for steam generation and hydrogen purification steps. The following sections describe the development of the component models needed to represent the baseline system configuration.

A. Solid-gas reactor

Coupled mass, species, and energy balance equations for the solid-gas reactor capture both the reduction and oxidation of the metal-oxide. Therefore, a single solid-gas reactor model is used for both the solar and water splitting reactors where the gas phase composition and operating temperature will determine the extent of the oxidation or reduction reaction. The chemistry of the solid metal-oxide is included in the reactor model as function calls.

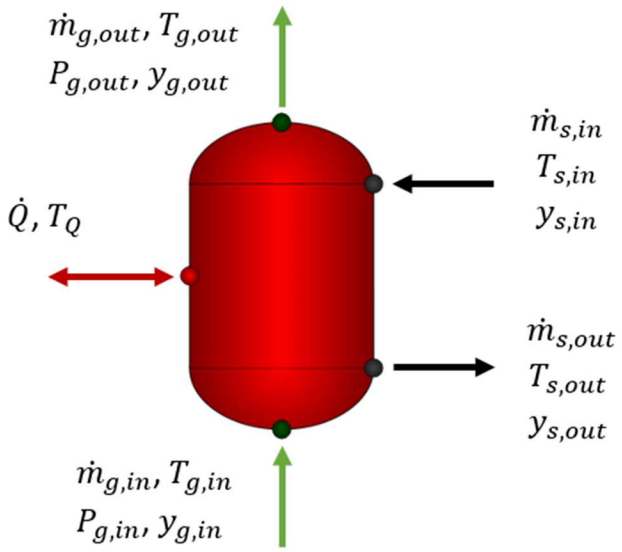

FIG. 3. Flow diagram of the solid gas reactor.

The mass balance equations for the solid and gas phases are given by equations (3) and (4). The equations are coupled through the solid-gas reaction term $\dot{m}_{ox}$ which allows for mass to be transfer between the phases. The species balance equation for oxygen in the gas phase is given in equation (5), which captures the change in composition due to solid gas reaction as well as homogenous gas phase reaction. Finally, the energy balance for the combined solid and gas phases is given by equation (6), which assumes the gas and solid phases thermally equilibrate in the reactor.

$$\dot{m}_{g,in} = \dot{m}_{g,out} - \dot{m}_{ox} \quad (3)$$

$$\dot{m}_{s,in} = \dot{m}_{s,out} + \dot{m}_{ox} \quad (4)$$

$$\dot{m}_{g,in} y_{g,in} = \dot{m}_{g,out} y_{g,out} - \dot{m}_{ox} + M(O_2)\nu_{rxn,O_2}\dot{r} \quad (5)$$

$$\dot{Q}_{rec,in} + \dot{m}_{s,in} h_{s,in} + \dot{m}_{g,in} h_{g,in} = \dot{m}_{s,out} h_{s,out} + \dot{m}_{g,out} h_{g,out} \quad (6)$$

B. Heat exchanger

Heat exchangers for the solid and gas phases were developed to model both recuperation as well as heat rejection. This component is utilized to recuperate thermal energy in the cooling/heating of the metal oxide when transferring between the solar and water splitting reactors. The component is also used to reduce the temperature of the gas leaving the solar reactor prior to vacuum pumping to improve the efficiency of the vacuum pumping process. In addition, heat is recuperated from gas leaving the water splitting reactor to raise the temperature of the entering gas. The heat exchangers are assumed to be in counter-flow configuration with a constant effectiveness (ε_{HX}) of 90%. The energy balance equations and effectiveness metric are given by equations (7) to (10).

$$\varepsilon_{HX} = \frac{Q_{HX}}{Q_{HX,max}} \quad (7)$$

$$Q_{HX,max} = min\left(\dot{m}_{in,2} C_p \left(T_{in,1} - T_{in,2}\right), \dot{m}_{in,1} C_p \left(T_{in,1} - T_{in,2}\right)\right) \quad (8)$$

$$Q_{HX} = \dot{m}_{in,2}\left(h_{out,2} - h_{in,2}\right) \quad (9)$$

$$Q_{HX} = \dot{m}_{in,1}\left(h_{in,1} - h_{out,1}\right) \quad (10)$$

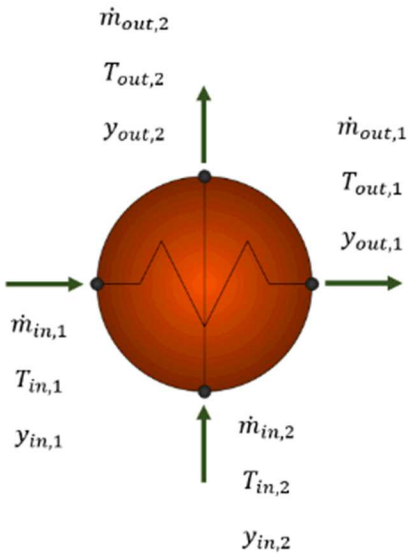

FIG. 4. General flow diagram for gas and solid heat exchangers.

C. Turbo machinery

The vacuum pump and blower models provide performance metrics for determining the electrical energy consumption to change the pressure of a gas flow stream.

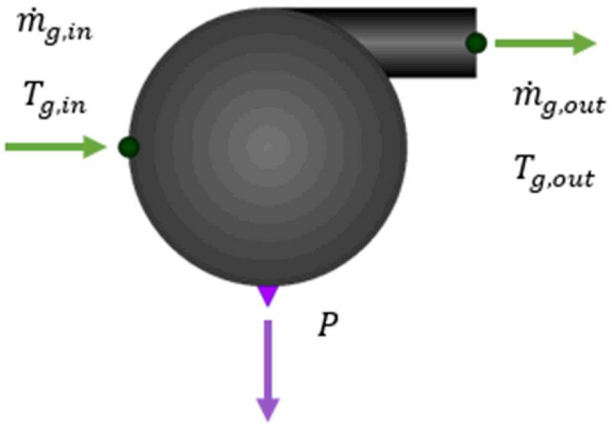

FIG. 5. Flow diagram of the turbo machinery. Vacuum pump and blower motor have the diagram view.

A vacuum pump is used to lower the pressure of the solar reduction receiver, which increases the degree of reduction at a given temperature. In the present model the vacuum pump is modeled as

an isothermal reversible process. The shaft power and energy balance are given below in equations (11) and (12), respectively.

$$\dot{W}_s = \dot{m}_g T_{g,in} \frac{\left(s_{g,out} - s_{g,in}\right)}{\eta_{pump}} \tag{11}$$

$$\dot{Q} = \dot{W}_s + \dot{m}_g\left(h_{g,in} - h_{g,out}\right) \tag{12}$$

The blower was modeled by the equations (13) and (14).

$$\dot{W}_s = \frac{\dot{m}_g}{\rho_{g,in}} \times \frac{P_{g,out} - P_{g,in}}{\eta_{blower}} \tag{13}$$

$$\dot{W}_s = \dot{m}_g\left(h_{g,out} - h_{g,in}\right) \tag{14}$$

D. Radiation heat transfer

In order to calculate the overall system efficiency, the efficiency of collecting solar energy at high temperature needs to be incorporated. The radiation heat transfer calculation can be linked to the thermal input of the solar reactor where the metal oxide particles are assumed to be directly irradiated and behave as a diffuse grey surface. The radiation heat transfer model is given by equations (15) to (18). The series of equations relates the irradiation incident on the receiver aperture from the heliostat field to the net thermal energy captured in the metal oxide material (Q_{rec}).

$$Q_{rerad} = \varepsilon_s \sigma A_{ap} T_{SR}^4 \tag{15}$$

$$Q_{reflect} = (1 - \varepsilon_s) Q_{irr} \tag{16}$$

$$Q_{conv} = A_{ap} h_{conv} (T_{SR} - T_o) \tag{17}$$

$$Q_{rec} = C\ DNI\ A_{ap} - \left(Q_{rerad} + Q_{reflect} + Q_{conv}\right) \tag{18}$$

III. Material Thermodynamics

OpenModelica allows for functions to be made and called within components. Therefore, a media section was defined in the model for the implementation of the metal oxide thermodynamic data. As a benchmark, ceria thermodynamic data was used for model development and to create the system modeling results. However, new material thermodynamic data can be implemented by defining functions that return the solid non-stoichiometry as a function of temperature and oxygen partial pressure $\left(\delta = f\left(T, P_{O_2}\right)\right)$ and the enthalpy of the solid-gas reaction as a function of non-stoichiometry $\left(\Delta H_{rxn} = f(\delta)\right)$.

For the modeling results presented in this paper, ceria thermodynamics were implemented based on the work of Bulfin et al.[4] The oxygen non-stoichiometry can be determined by solving equation (19) for δ. The dependence on both the temperature and oxygen partial pressure can be observed in FIG. 6 where multiple isotherms are plotted as a function of oxygen partial pressure. In the system model, this equation must be solved in conjunction with the gas and solid species as well as energy balance such that the reaction extent is constrained by thermochemical equilibrium.

$$\left(\frac{\delta}{0.35-\delta}\right) = 8700{P_{O_2}}^{-0.217} exp\left(\frac{-195.6 kJmol^{-1}}{RT}\right) \tag{19}$$

The enthalpy of the solid-gas reaction as a function of oxygen non-stoichiometry can be calculated according to equation (20). However, in the system model it is desirable to convert this value into solid enthalpy by integrating the reaction enthalpy as a function of oxygen non-stoichiometry and combining with the sensible term $\left(h_s = \frac{1}{M_{MO_{x-\delta}}}\left[\int_{\delta_o}^{\delta} \Delta \mathrm{H_{rxn}}\, d\delta + \int_{T_o}^{T} c_p\, dT\right]\right)$.

$$\Delta H_{rxn} = (478 - 1158\delta + 1790\delta^2 + 23368\delta^3 - 64929\delta^4) \times 10^3 \tag{20}$$

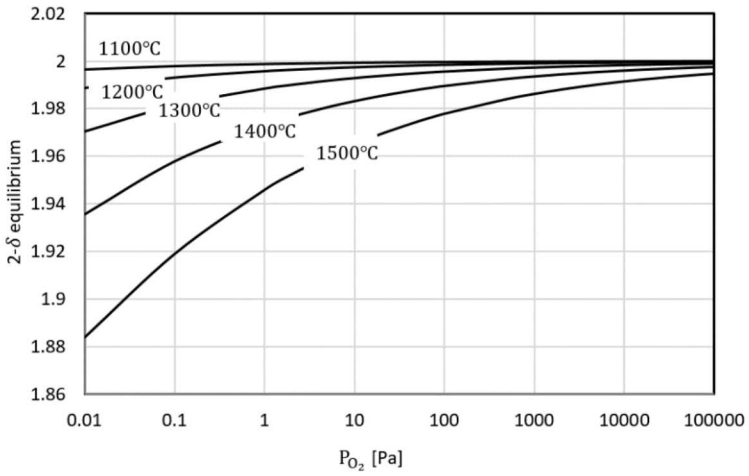

FIG. 6. Equilibrium vacancy concentration for ceria as a function of temperature and oxygen partial pressure.

IV. System Modeling Results

From the development of the components in the modeling approach section along with the material thermodynamics of ceria, the system can be configured and simulated for a given set of operating conditions. The full system in the OpenModelica environment is shown in FIG. 7. For

the model to be fully defined, sources and sinks contain the boundary conditions of the system and performance metrics for the individual components need to be specified.

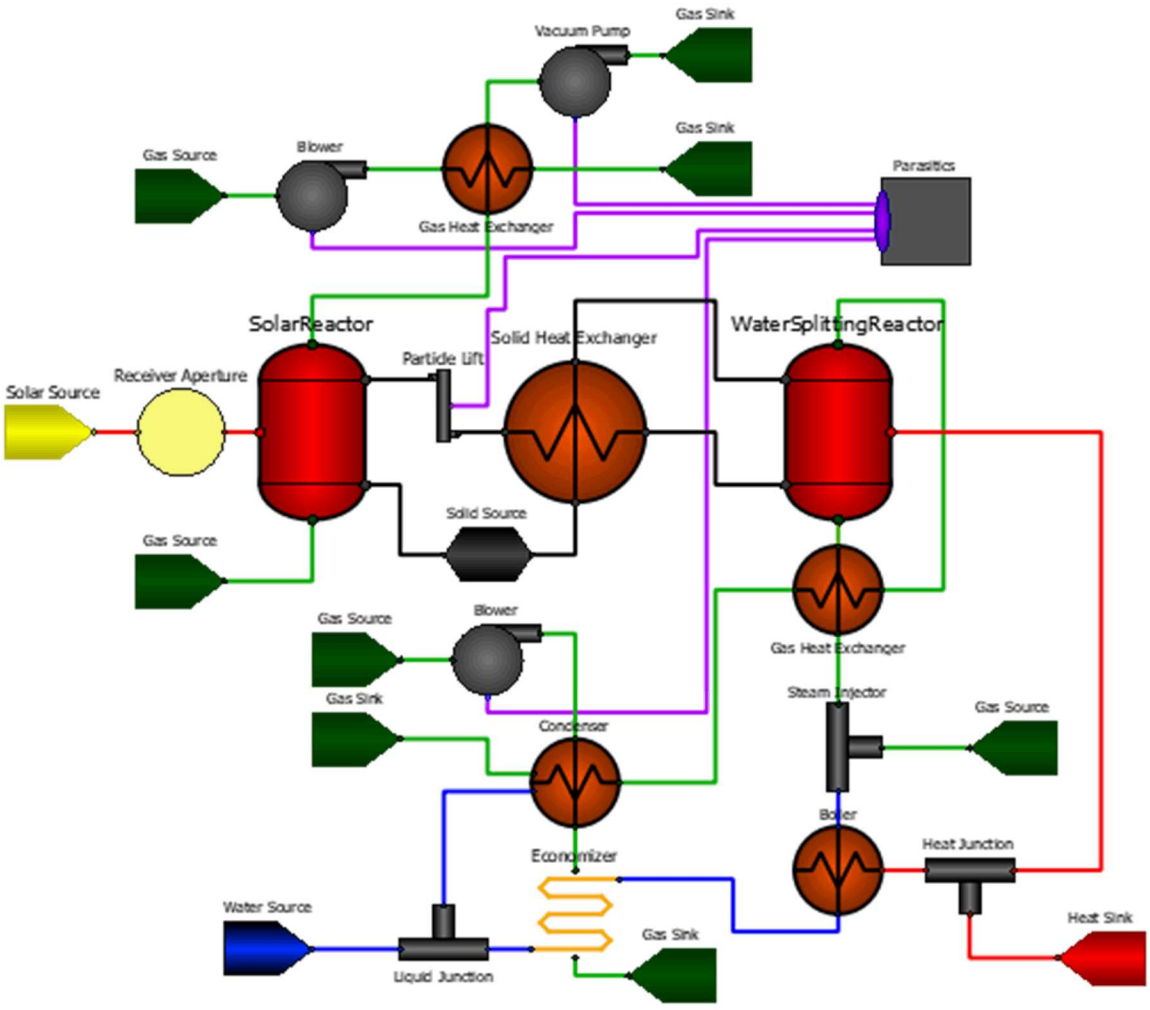

FIG. 7. Diagram view of OpenModelica component based system level model.

Parametric studies of the system performance as a function of the operating conditions were conducted by developing a script written in the OpenModelica Shell. The script varies the temperature of the water splitting reactor with the solar reactor fixed at 1500 °C. The water splitting reactor temperature was varied from 1500 °C (isothermal operation) to 1100 °C with solar reactor pressures between 1 and 100 Pa. The efficiency of the system is calculated for each simulation according to equation (21). The numerator represents the rate of hydrogen production multiplied

by the heating value while the denominator is the overall thermal power required by the system, which is inclusive of the solar thermal input and the electrical parasitics assuming a 40% thermal-to-electric conversion.

$$\eta = \frac{y_{H_2}\dot{m}_{g,out}\Delta H_{HV}}{\left(Q_{in} + \frac{\sum P}{0.4}\right)} \tag{21}$$

The results of the system parametric studies are plotted in FIG. 8, which illustrates the dependence of system-level solar-to-hydrogen efficiency on the operating temperature of the water splitting reactor and pressure of the solar reactor for ceria. Peak efficiencies are observed for each of the isobars at a given temperature difference. Inefficiencies at low temperature difference are primarily due to low steam conversion at high temperature in the water splitting reactor. As the temperature difference between the water splitting and solar reduction reactor is increased the additional heat is required by the receiver to increase the temperature of the ceria and the steam conversion improves. However, the water splitting reactor will eventually shift from a net heat rejection to requiring an additional heat input. The requirement for an additional heat input causes the efficiency to drop off at low water splitting reactor temperatures. The peak efficiency values at the different solar reactor pressures are given in

.

Table 1: Optimal temperature swing between the solar and water splitting reactor at various solar reactor operating pressures.

Pressure [Pa]	**Change in Temperature [℃]**	**Efficiency [%]**
1	251.85	25.8342
3	290.85	23.9486
10	332.85	21.6754
20	356.85	20.2816
50	383.85	18.4359
100	401.85	17.0297

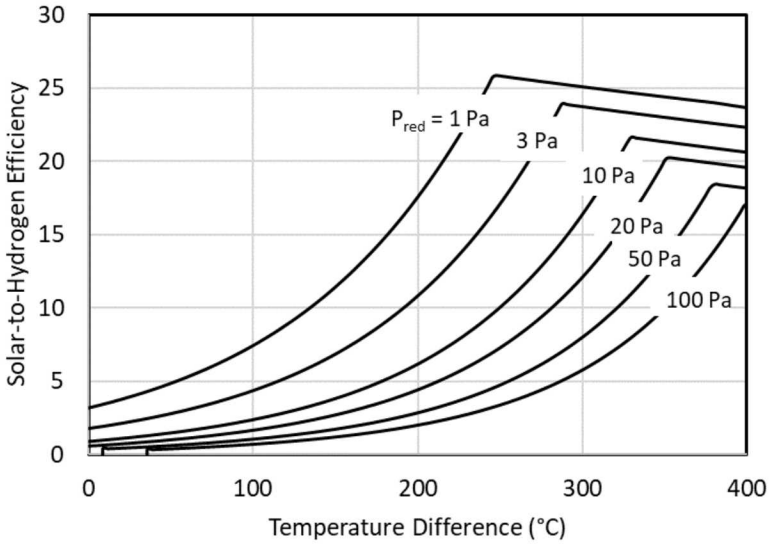

FIG. 8. Solar-to-hydrogen efficiency as a function of temperature swing between the solar and water splitting reactor at various solar reactor operating pressures.

V. CONCLUSION

An object-oriented modeling approach for solar-to-hydrogen efficiency calculations was developed and implemented in the OpenModelica environment. This tool allows for new material thermodynamics to be incorporated for system-level solar-to-hydrogen efficiency calculations as well as reconfiguration and replacement of component models with ease. However, a more robust initialization procedure is needed to make the STCH model stable over the entire operating envelope. As a benchmark for the model, ceria thermodynamic properties were implemented. Simulations achieved a maximum efficiency of 25.83% at 1 Pa and a temperature difference of 251.85℃. Further work should include the use of OMOptim which is a sub-system of OpenModelica that allows for design optimization. Parameter and configuration optimization can be achieved in OMOptim. This will allow for optimal components and connection paths to be used in a model.[7]. Such a study has the potential to increase the solar-to-hydrogen efficiency.

Nomenclature			
δ	equilibrium vacancy concentration	P	parasitic power (W)
R	ideal gas constant (J mol^{-1} K^{-1})	P_g	gas pressure (Pa)
P_{O_2}	oxygen partial pressure (Bar)	y_g	gas mass fraction
$\dot{m}_s$	solid mass flow rate (kg s^{-1})	y_s	solid mass fraction
$\dot{m}_g$	gas mass flow rate (kg s^{-1})	q_f	heat flux (W m^2)
T	temperature (K)	$\dot{Q}_{rec}$	heat flow (W)
ε_{HX}	Effectiveness	h	specific enthalpy (J kg^{-1})
C_p	specific heat capacity (J kg^{-1} K^{-1})	ΔH_{rxn}	change in enthalpy for reduction (J)
s	specific entropy (J kg^{-1} K^{-1})	ρ	density (kg m^{-3})
$\dot{W}_s$	shaft power (W)	η	efficiency
ΔH_V	hydrogen heat value 119,953,000 (J kg^{-1})	$M(O_2)$	oxygen molar mass (kg mol^{-1})
ν_{rxO_2}	oxygen equilibrium constant	$\dot{r}$	reaction rate (mol s^{-1})
ε_s	solid emissivity	σ	Stephan-Boltzmann constant
A_{ap}	aperture area (m^2)	h_{conv}	convective heat loss (W m^{-2} K^{-1})
C	concentration ratio	DNI	direct normal insolation (W m^{-2})

Acknowledgements

This work was supported in part by the U.S Department of Energy, Office of Science, Office of Workforce Development for Teachers and Scientists (WDTS) under the Science Undergraduate Laboratory Internship (SULI) program.

This material is based upon work supported by the U.S. Department of Energy, Office of Energy Efficiency and Renewable Energy (EERE), specifically the Fuel Cell Technologies Office.

Sandia National Laboratories is a multimission laboratory managed and operated by National Technology & Engineering Solutions of Sandia, LLC, a wholly owned subsidiary of Honeywell International Inc., for the U.S. Department of Energy's National Nuclear Security Administration under contract DE-NA0003525.

References

[1] K. Albrecht, G. Jackson, R. Braun, "Evaluating thermodynamic performance limits of thermochemical energy storage subsystems using reactive perovskite oxide particles for concentrating solar power," *Solar Energy.* 167, 179-193 (2018).

[2]B. Bulfin, F. Call, M. Lange, O. Luebben, C. Sattler, R. Pitz-Paal, I.V. Shvets, "Thermodynamics of CeO_2 Thermochemical Fuel Production," *Energy Fuels.* 29 (2), 1001-1009 (2015).

[3]R. Panlener, R. Blumenthal, J. J Garnier, "A thermodynamic study of nonstoichiometric cerium dioxide," Phys. Chem. Solids, 36, 1213-1222 (1975).

[4]B. Bulfin, A. J. Lowe, K. A. Keogh, B. E. Murphy, O. Lubben, S. A. Krasnikov, I. V. Shvets, "Analytical Model of CeO_2 Oxidation and Reduction," J. Phys. Chem. C, 117, 46, 24129-24137 (2013).

[5]B. Bulfin, J. Vieten, C. Agrafiotis, M. Roeb, C. Sattler, "Applications and limitations of two step metal oxide thermochemical redox cycles; a review," J. Mater. Chem. A, 5, 18951-18966 (2017).

[6]S. Brendelberger, M. Roeb, M. Lange, C. Sattler, "Counter flow sweep gas demand for the ceria redox cycle," *Solar Energy.* 122, 1011-1022 (2013).

[7]H. Thieriot, M. Nemer, M. Torabzadeh-Tari, P. Fritzson, R. Singh, J.J Kocherry, "Towards design optimization with OpenModelica emphasizing parameter optimization with genertic algorithms," Proceedings 8th Modelica Conference, Dresden, Germany, (2011).